BULLETIN OF THE POLISH ACADEMY OF SCIENCES
TECHNICAL SCIENCES, Vol. 65, No. 6, 2017
DOI: 10.1515/bpasts-2017-0092

Iterative sliding mode observer for sensorless control of five-phase permanent magnet synchronous motor

J. YANG*, M. DOU, and D. ZHAO

School of Automation, Northwestern Polytechnical University, Xi'an 710072, China

Abstract. Due to the star connection of the windings, the impact of the third harmonic which does not exist in three-phase permanent magnet synchronous motor (PMSM) cannot be ignored in five-phase PMSM. So the conventional sensorless control methods for three-phase PMSM cannot be applied for five-phase PMSM directly. To achieve the sensorless control for five-phase PMSM, an iterative sliding mode observer (ISMO) is proposed with the consideration of the third harmonic impact. First, a sliding mode observer (SMO) is designed based on the five-phase PMSM model with the third harmonic to reduce the chattering and obtain the equivalent signal of the back electromotive force (EMF). Then, an adaptive back EMF observer is built to estimate the motor speed and rotor position, which eliminates the low-pass filter and phase compensation module and improves the estimation accuracy. Meanwhile, by iteratively using the SMO in one current sampling period to adjust the sliding mode gains, the sliding mode chattering and estimation errors of motor speed and rotor position are further reduced. Besides, the stability of the SMO and the adaptive back EMF observer are demonstrated in detail by Lyapunov stability criteria. Experiment results verify the effectiveness of the proposed observer for sensorless control of five-phase PMSM.

Key words: five-phase PMSM, sensorless control, iterative sliding mode observer (ISMO), Lyapunov criteria, speed and position estimation.

1. Introduction

Owing to high torque-to-current ratio, large power-to-weight ratio, high efficiency, high power factor, high fault tolerance capability and robustness, five-phase permanent magnet synchronous motors (PMSMs) have gained more attention in high reliability and high fault tolerant applications such as electric vehicles, wind power generation, machine tools, robotics and aerospace [1–4]. Compared with the conventional three-phase PMSM, under the same rated power, since the phase number is increased in five-phase PMSM, the current of each phase is reduced without increasing the stator voltage, so the rating current of IGBT or other semiconductors in motor drive system can be lower. Meanwhile, with the increasing number of phase, the torque ripples are also reduced [5–7]. Besides, five-phase PMSM can be operated under the loss of one or two phases continuously; thus, the fault tolerance capability and the reliability are higher than the conventional three-phase PMSM. Based on these advantages, five-phase PMSMs are applied increasingly widely in drive control systems operated in harsh environment [8, 9].

In electric drive system of five-phase PMSM, the field oriented control method is a common used control technique with good performance in both steady and transient states [10]. The core concept of the field oriented control strategy is transforming the model of five-phase PMSM in natural coordinate system to decoupled equations in rotating coordinate system and controlling the five-phase PMSM as DC motor [10]. For the electric drive system of five-phase PMSM, the conventional control strategy usually needs the information of rotor position and speed for closed-loop control by position sensor such as an optical encoder fixed on the motor shaft [11]. Unfortunately, the position sensor, which is sensitive to the vibration and temperature, restricts the application of five-phase PMSM in electric drive system operated in harsh environmental conditions, and reduces the reliability of the whole electric drive system [12, 13].

Nowadays, with the development of digital signal processor [14–16], the sensorless control technology has gained more attention in drive control system of three-phase PMSM. The sensorless control techniques are generally divided into two categories which are the high-frequency signal injection method by utilizing the salient effect of PMSM [17–19] and the observer estimation method based on all kinds of observers [20–22]. Unfortunately, the high-frequency signal injection method depends on the saliency of the motor. So the application of this method is usually limited to interior PMSM. Besides, the high-frequency injection signal will bring high-frequency noise and cause the performance degradation in electric drive system. And the observer estimation methods such as model reference adaptive method [23, 24] and Kalman filtering method [25, 26] are dependent on an accurate model of the PMSM to a certain extent. However, for the good robustness, simple algorithm implementation and relative independence of the motor model, the sliding mode observer (SMO) [27–29] method is an effective rotor position estimation method used for sensorless control of three-phase PMSM widely.

*e-mail: yangjianwei100@hotmail.com

Manuscript submitted 2017-03-04, revised 2017-04-24, initially accepted for publication 2017-05-15, published in December 2017.

The SMO in sensorless control of three-phase PMSM is often designed by the errors between the estimated values of the stator phase currents estimated by the SMO in the stationary reference frame and the actual values of the stator phase currents obtained by the current sensor sampling to estimate the back EMF for the further estimation of the rotor velocity and position. In the conventional SMO, the sign function is utilized as the control function to build the current observer and obtain the equivalent signals of the back EMF. Unfortunately, due to the discreteness of the sign function, the conventional SMO always brings with serious chattering and the equivalent signal of the back EMF usually contains high frequency oscillation component seriously. So the low pass filters are usually needed to extract the required back EMF signals. However, the insertion of low pass filters causes the phase delay which is usually compensated by the additional phase compensation module. In order to solve the problem, an adaptive filter with an adaptive gain is proposed in [30] for sensorless control of three-phase PMSM, but it still unable to implement the phase compensation completely. In [31], to reduce the chattering of the SMO, the switching function of the SMO is designed by replacing the conventional sign function with the saturation function for the sensorless control in three-phase PMSM drive control system. Nevertheless, the reduction of the chattering in the SMO is not very obvious because the saturation function is still a discrete function. In [27], without using the sign function or the saturation function, the SMO is realized by employing the sigmoid function which is a continuous function as the control function and the chattering phenomenon in this SMO is reduced. In [28], a SMO with adaptive back EMF observer is discussed, which eliminates the low-pass filter and phase compensation module, and the estimation accuracy of the motor speed and angle are also enhanced in the sensorless control system. Unfortunately, both the SMOs in [27] and [28] are about sensorless control of three-phase PMSM. For sensorless control of five-phase PMSM, since unable to ignore the impact of the third harmonic, the items of the third harmonic current in the SMO must be considered, and the stability conditions analyzed by Lyapunov function are different from the SMOs in sensorless control of three-phase PMSM. So the SMO design for sensorless control of five-phase PMSM is more complex and the references about SMO for sensorless control of five-phase PMSM are fewer.

In this paper, an iterative sliding mode observer (ISMO) is proposed for sensorless control of five-phase PMSM in electric drive system with the consideration of the third harmonic impact. A SMO is designed firstly based on the five-phase PMSM model with the third harmonic to reduce the chattering and obtain the equivalent signal of the back EMF. Then, an adaptive back EMF observer is built to estimate the rotor speed and position of five-phase PMSM, which eliminates the low-pass filter and phase compensation module and improves the estimation accuracy. Meanwhile, by iteratively using the SMO in one current sampling period to adjust the sliding mode gains, the sliding mode chattering and estimation errors of rotor speed and position are further reduced. Besides, the stability of the designed SMO and the adaptive back EMF observer are proved in detail by Lyapunov stability criteria.

2. Mathematical model of five-phase PMSM

To achieve the sensorless control of five-phase PMSM in electric drive system, the five-phase PMSM model is established firstly. Without loss of generality, the assumptions are as follows. Firstly, the magnetic circuit is linear. It means that the magnetic circuit is not saturable. Secondly, the five-phase PMSM is surface mounted non-salient pole structure. Thirdly, the slot effect of stator and rotor surface is neglected. Fourthly, the motor inductance change caused by uneven air gap is ignored. Fifthly, the eddy currents and the hysteresis losses are negligible. Sixthly, the stator winding is symmetrical. It means the even harmonics can be canceled mutually. Lastly, just consider the impact of third harmonic and ignore the effects of other high-order harmonics. By the assumptions above, the five-phase PMSM model in the natural coordinate system is shown as [32]:

$$\boldsymbol{U_s} = \boldsymbol{R_s}\boldsymbol{I_s} + \frac{d\boldsymbol{\psi_s}}{dt} \tag{1}$$

$$\boldsymbol{\psi_s} = \boldsymbol{L_s}\boldsymbol{I_s} + \boldsymbol{\psi_m} \tag{2}$$

$$T_e = \frac{\partial W}{\partial \theta} = P\left[\frac{1}{2}\boldsymbol{I_s^T}\frac{\partial \boldsymbol{L_s}}{\partial \theta}\boldsymbol{I_s} + I_s\frac{\partial \boldsymbol{\psi_m}}{\partial \theta}\right] \tag{3}$$

$$T_e - T_L = J\frac{d\omega}{dt} + B\omega \tag{4}$$

where (1) is the voltage balance equation, (2) is the flux equation, (3) is the torque equation and (4) is the mechanical motion equation. And the stator phase voltage vector $\boldsymbol{U_s} = [U_a\ U_b\ U_c\ U_d\ U_e]^T$; the stator phase current vector $\boldsymbol{I_s} = [i_a\ i_b\ i_c\ i_d\ i_e]^T$; the stator winding resistance $\boldsymbol{R_s} = R_s \times \boldsymbol{I}_{5\times5}$, the stator flux vector $\boldsymbol{\Psi_s} = [\Psi_a\ \Psi_b\ \Psi_c\ \Psi_d\ \Psi_e]^T$; Ψm is the rotor flux vector; $\boldsymbol{L_s}$ is the stator inductance matrix; P is the number of pole pairs; and T_e is the electromagnetic torque; T_L is the load torque; J is the rotational inertia; B is the viscous friction coefficient; ω is the mechanical angular velocity.

Compared to conventional three-phase PMSM, due to the addition of two phase windings, the stator inductance matrix $\boldsymbol{L_s}$ of five-phase PMSM is relatively complex and can be expressed as:

$$\begin{aligned}\boldsymbol{L_s} = {} & L_{ls} \times \boldsymbol{I}_{5\times5} + \\ & + L_{m1}\begin{bmatrix} 1 & \cos\alpha & \cos2\alpha & \cos3\alpha & \cos4\alpha \\ \cos\alpha & 1 & \cos\alpha & \cos2\alpha & \cos3\alpha \\ \cos2\alpha & \cos\alpha & 1 & \cos\alpha & \cos2\alpha \\ \cos3\alpha & \cos2\alpha & \cos\alpha & 1 & \cos\alpha \\ \cos4\alpha & \cos3\alpha & \cos2\alpha & \cos\alpha & 1 \end{bmatrix} + \\ & + L_{m3}\begin{bmatrix} 1 & \cos3\alpha & \cos6\alpha & \cos9\alpha & \cos12\alpha \\ \cos3\alpha & 1 & \cos3\alpha & \cos6\alpha & \cos9\alpha \\ \cos6\alpha & \cos3\alpha & 1 & \cos3\alpha & \cos6\alpha \\ \cos9\alpha & \cos6\alpha & \cos3\alpha & 1 & \cos3\alpha \\ \cos12\alpha & \cos9\alpha & \cos6\alpha & \cos3\alpha & 1 \end{bmatrix}\end{aligned} \tag{5}$$

where L_{ls} is the leakage inductance of each phase winding; L_{m1} is the self-inductance of fundamental wave phase winding A (B, C, D, E); L_{m3} is the self-inductance of third harmonic phase winding A (B, C, D, E) and $\alpha = 72°$.

And the rotor flux vector of five-phase PMSM $\boldsymbol{\Psi_m}$ is also more complex than the three-phase PMSM. The rotor flux vector of five-phase PMSM is shown as

$$\boldsymbol{\psi_m} = \psi_{m1}\begin{bmatrix}\cos\theta\\ \cos(\theta-\alpha)\\ \cos(\theta-2\alpha)\\ \cos(\theta-3\alpha)\\ \cos(\theta-4\alpha)\end{bmatrix} + \psi_{m3}\begin{bmatrix}\cos 3\theta\\ \cos 3(\theta-\alpha)\\ \cos 3(\theta-2\alpha)\\ \cos 3(\theta-3\alpha)\\ \cos 3(\theta-4\alpha)\end{bmatrix} \tag{6}$$

where Ψ_{m1} is the flux amplitude of fundamental wave; Ψ_{m3} is the flux amplitude of third harmonic and θ is the rotor electrical angle.

For controlling the five-phase PMSM as DC motor, the five-phase PMSM model in the natural coordinates system should be transformed to the model in the rotating coordinate system. The five-phase PMSM model with the third harmonic in the rotating coordinate system d1-q1-d3-q3 is shown as below:

$$\begin{bmatrix}u_{d1}\\ u_{q1}\\ u_{d3}\\ u_{q3}\end{bmatrix} = R_s\begin{bmatrix}i_{d1}\\ i_{q1}\\ i_{d3}\\ i_{q3}\end{bmatrix} + p\begin{bmatrix}L_{d1}&0&0&0\\ 0&L_{q1}&0&0\\ 0&0&L_{d3}&0\\ 0&0&0&L_{q3}\end{bmatrix}\begin{bmatrix}i_{d1}\\ i_{q1}\\ i_{d3}\\ i_{q3}\end{bmatrix} + \omega_e\begin{bmatrix}-L_{q1}i_{q1}\\ L_{d1}i_{d1}\\ -3L_{q3}i_{q3}\\ 3L_{d3}i_{d1}\end{bmatrix} + \omega_e\begin{bmatrix}0\\ \psi_{m1,q1}\\ 0\\ \psi_{m3,q3}\end{bmatrix} \tag{7}$$

$$T_e = \frac{5}{2}P\left[\psi_{m1,q1}i_{q1} + 3\psi_{m3,q1}i_{q3}\right] \tag{8}$$

where (7) is the voltage balance equation; (8) is the torque equation; $[u_{d1}\ u_{q1}\ u_{d3}\ u_{q3}]^{\mathrm{T}}$ is the stator phase voltage vector; $[i_{d1}\ i_{q1}\ i_{d3}\ i_{q3}]^{\mathrm{T}}$ is the stator phase current vector; $diag(L_{d1}\ L_{q1}\ L_{d3}\ L_{q3})$ is the stator inductance matrix; $[0\ \Psi_{m1,q1}\ 0\ \Psi_{m1,q3}]^{\mathrm{T}}$ is the rotor flux vector; ω_e is the electrical angular velocity; $p = d/dt$ is the differential operator. And since the motor is surface mounted non-salient pole structure, $L_{d1} = L_{q1} = L_{ls} + 2.5L_{m1}$, $L_{d3} = L_{q3} = L_{ls} + 2.5L_{m3}$. The coordinate transformation matrix is shown as follow:

$$T(\theta) = \frac{2}{5}\begin{bmatrix}\cos\theta & \cos(\theta-\frac{2\pi}{5}) & \cos(\theta-\frac{4\pi}{5}) & \cos(\theta+\frac{4\pi}{5}) & \cos(\theta+\frac{2\pi}{5})\\ -\sin\theta & -\sin(\theta-\frac{2\pi}{5}) & -\sin(\theta-\frac{4\pi}{5}) & -\sin(\theta+\frac{4\pi}{5}) & -\sin(\theta+\frac{2\pi}{5})\\ \cos\theta & \cos(\theta+\frac{4\pi}{5}) & \cos(\theta-\frac{2\pi}{5}) & \cos(\theta+\frac{2\pi}{5}) & \cos(\theta-\frac{4\pi}{5})\\ -\sin\theta & -\sin(\theta+\frac{4\pi}{5}) & -\sin(\theta-\frac{2\pi}{5}) & -\sin(\theta+\frac{2\pi}{5}) & -\sin(\theta-\frac{4\pi}{5})\\ \frac{1}{2} & \frac{1}{2} & \frac{1}{2} & \frac{1}{2} & \frac{1}{2}\end{bmatrix} \tag{9}$$

For sensorless control of five-phase PMSM, the five-phase PMSM model in the stationary reference frame is also needed. The five-phase PMSM model in the stationary reference frame α1-β1-α3-β3 is shown as

$$\begin{bmatrix}u_{\alpha1}\\ u_{\beta1}\\ u_{\alpha3}\\ u_{\beta3}\end{bmatrix} = R_s\begin{bmatrix}i_{\alpha1}\\ i_{\beta1}\\ i_{\alpha3}\\ i_{\beta3}\end{bmatrix} + p\begin{bmatrix}L_{\alpha1}&0&0&0\\ 0&L_{\beta1}&0&0\\ 0&0&L_{\alpha3}&0\\ 0&0&0&L_{\beta3}\end{bmatrix}\begin{bmatrix}i_{\alpha1}\\ i_{\beta1}\\ i_{\alpha3}\\ i_{\beta3}\end{bmatrix} + \begin{bmatrix}e_{\alpha1}\\ e_{\beta1}\\ e_{\alpha3}\\ e_{\beta3}\end{bmatrix} \tag{10}$$

where $[u_{\alpha1}\ u_{\beta1}\ u_{\alpha3}\ u_{\beta3}]^{\mathrm{T}}$ is the stator phase voltage vector; $[i_{\alpha1}\ i_{\beta1}\ i_{\alpha3}\ i_{\beta3}]^{\mathrm{T}}$ is the stator phase current vector; $diag(L_{\alpha1}\ L_{\beta1}\ L_{\alpha3}\ L_{\beta3})$ is the equivalent stator inductance matrix; $[e_{\alpha1}\ e_{\beta1}\ e_{\alpha3}\ e_{\beta3}]^{\mathrm{T}}$ is the back EMF vector. And since the motor is surface mounted non-salient pole structure, $L_{d1} = L_{q1} = L_{\alpha1} = L_{\beta1}$, $L_{d3} = L_{q3} = L_{\alpha3} = L_{\beta3}$. The coordinate transformation matrix is shown as follows:

$$\boldsymbol{C}_{s/r} = \begin{bmatrix}\cos\theta & \sin\theta & 0 & 0 & 0\\ -\sin\theta & \cos\theta & 0 & 0 & 0\\ 0 & 0 & \cos 3\theta & \sin 3\theta & 0\\ 0 & 0 & -\sin 3\theta & \cos 3\theta & 0\\ 0 & 0 & 0 & 0 & 1\end{bmatrix}. \tag{11}$$

3. Iterative sliding mode observer design

The overall block diagram of sensorless control system for five-phase PMSM based on SMO method is shown in Fig. 1.

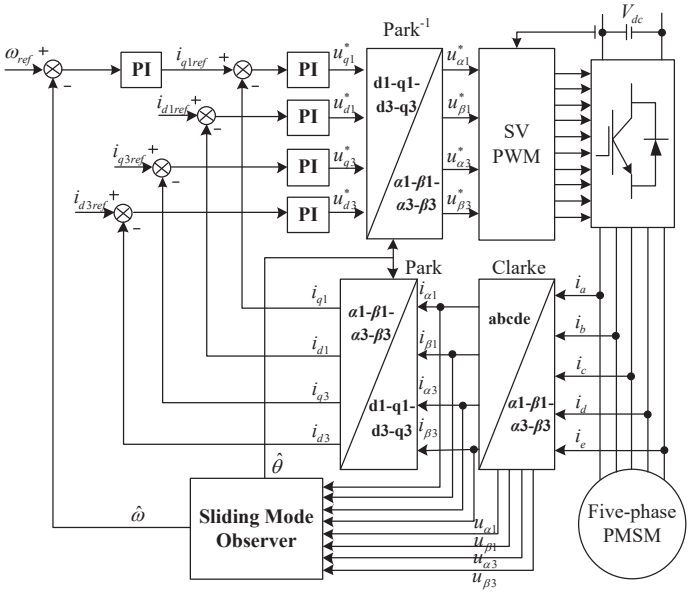

Fig. 1. Block diagram of SMO sensorless control system for five-phase PMSM

It is noticed that the sensorless control system of five-phase PMSM based on SMO method has the similarities with the one of three-phase PMSM. Both of the sensorless control systems for two kinds of PMSM are often adopted the PI control strategy [33, 34]. And the coordinate transform and inverse coordinate transform are commonly used for the decoupling control in the two of different PMSM control systems. Besides, the SMO which is used for observing the motor speed and the rotor position is the core to achieve the sensorless control for both of three-phase PMSM and five-phase PMSM. Of course, there are differences between the sensorless control systems of three-phase PMSM and five-phase PMSM. Because the impact of the third harmonic is unable to ignore, the third harmonic voltage and current should also be considered in the SMO for sensorless control of five-phase PMSM. So the SMO in the sensorless control system of five-phase PMSM is more complex relatively than the one of three-phase PMSM.

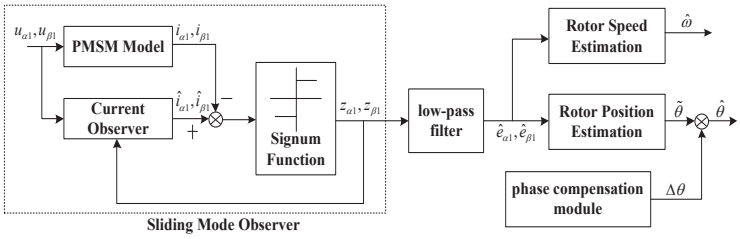

Fig. 2. Block diagram of conventional SMO for sensorless control of three-phase PMSM

The block diagram of conventional SMO for sensorless control of three-phase PMSM is shown as Fig. 2. It can be seen that the conventional SMO usually contains the SMO, low-pass filter, phase compensation module and rotor speed and position estimation unit. Besides, the conventional SMO is only considered with the fundamental wave. And as the sign function in the SMO is a discrete function, the low-pass filter is indispensable in the sensorless control system to reduce the serious chattering and filter out the high frequency signal. The phase compensation module is also essential to reduce the phase delay caused by the low-pass filter.

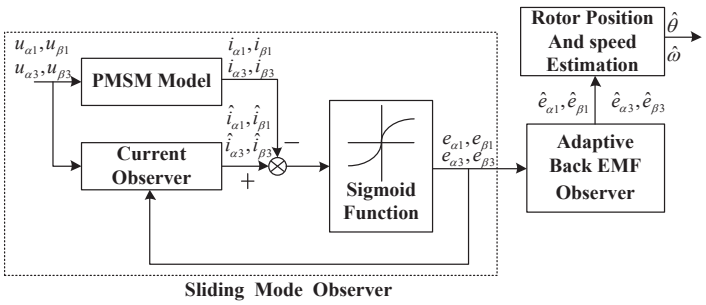

Fig. 3. Block diagram of SMO for sensorless control of five-phase PMSM

The SMO for five-phase PMSM sensorless control is designed as Fig. 3. It is different from the SMO in sensorless control system of three-phase PMSM. The SMO is considered with third harmonic voltage and current and the switching function in the SMO is the sigmoid function. As the sigmoid function is a continuous function, the chattering phenomenon in the SMO is reduced. And by use of the adaptive back EMF observer after the SMO, the low-pass filter and phase compensation module which are indispensable in the conventional SMO are eliminated. So the structure of the SMO for sensorless control of five-phase PMSM is relatively simple.

3.1. Sliding mode observer design. Based on the five-phase PMSM model (10) in the stationary reference frame α1-β1-α3-β3 described before, the current state equation of five-phase PMSM in the stationary reference frame α1-β1-α3-β3 can be rewritten as:

$$\begin{cases} \dfrac{di_{\alpha1}}{dt} = -\dfrac{R_s}{L_{\alpha1}} i_{\alpha1} + \dfrac{1}{L_{\alpha1}} u_{\alpha1} - \dfrac{1}{L_{\alpha1}} e_{\alpha1} \\ \dfrac{di_{\beta1}}{dt} = -\dfrac{R_s}{L_{\beta1}} i_{\beta1} + \dfrac{1}{L_{\beta1}} u_{\beta1} - \dfrac{1}{L_{\beta1}} e_{\beta1} \\ \dfrac{di_{\alpha3}}{dt} = -\dfrac{R_s}{L_{\alpha3}} i_{\alpha3} + \dfrac{1}{L_{\alpha3}} u_{\alpha3} - \dfrac{1}{L_{\alpha3}} e_{\alpha3} \\ \dfrac{di_{\beta3}}{dt} = -\dfrac{R_s}{L_{\beta3}} i_{\beta3} + \dfrac{1}{L_{\beta3}} u_{\beta3} - \dfrac{1}{L_{\beta3}} e_{\beta3}. \end{cases} \tag{12}$$

And based on the current state equation (12) and the sliding mode variable structure theory, the SMO can be preliminarily designed as:

$$\begin{cases} \dfrac{d\hat{i}_{\alpha1}}{dt} = -\dfrac{R_s}{L_{\alpha1}} \hat{i}_{\alpha1} + \dfrac{1}{L_{\alpha1}} u_{\alpha1} - \dfrac{k_1}{L_{\alpha1}} sgn(\hat{i}_{\alpha1} - i_{\alpha1}) \\ \dfrac{d\hat{i}_{\beta1}}{dt} = -\dfrac{R_s}{L_{\beta1}} \hat{i}_{\beta1} + \dfrac{1}{L_{\beta1}} u_{\beta1} - \dfrac{k_1}{L_{\beta1}} sgn(\hat{i}_{\beta1} - i_{\beta1}) \\ \dfrac{d\hat{i}_{\alpha3}}{dt} = -\dfrac{R_s}{L_{\alpha3}} \hat{i}_{\alpha3} + \dfrac{1}{L_{\alpha3}} u_{\alpha3} - \dfrac{k_2}{L_{\alpha3}} sgn(\hat{i}_{\alpha3} - i_{\alpha3}) \\ \dfrac{d\hat{i}_{\beta3}}{dt} = -\dfrac{R_s}{L_{\beta3}} \hat{i}_{\beta3} + \dfrac{1}{L_{\beta3}} u_{\beta3} - \dfrac{k_2}{L_{\beta3}} sgn(\hat{i}_{\beta3} - i_{\beta3}) \end{cases} \tag{13}$$

where $[\hat{i}_{\alpha1}\ \hat{i}_{\beta1}\ \hat{i}_{\alpha3}\ \hat{i}_{\beta3}]^T$ is the estimated current value of the SMO; $[u_{\alpha1}\ u_{\beta1}\ u_{\alpha3}\ u_{\beta3}]^T$ is the actual value of the voltage; $[i_{\alpha1}\ i_{\beta1}\ i_{\alpha3}\ i_{\beta3}]^T$ is the actual value of current measured by current sensor and transformed by coordinate transformation matrix; k_1 and k_2 are the gains of the SMO; $sgn(x)$ represents the sign function which is the switching function in the SMO.

Equation (13) is the conventional SMO for sensorless control of five-phase PMSM. However, due to the discreteness of the sign function, the performance of the SMO above-men-

tioned is not very good. The new SMO for five-phase PMSM SMO sensorless control system is further designed as

$$\begin{cases} \dfrac{d\hat{i}_{\alpha 1}}{dt} = -\dfrac{R_s}{L_{\alpha 1}}\hat{i}_{\alpha 1} + \dfrac{1}{L_{\alpha 1}}u_{\alpha 1} - \dfrac{k_1}{L_{\alpha 1}}sig\left(\hat{i}_{\alpha 1} - i_{\alpha 1}\right) \\ \dfrac{d\hat{i}_{\beta 1}}{dt} = -\dfrac{R_s}{L_{\beta 1}}\hat{i}_{\beta 1} + \dfrac{1}{L_{\beta 1}}u_{\beta 1} - \dfrac{k_1}{L_{\beta 1}}sig\left(\hat{i}_{\beta 1} - i_{\beta 1}\right) \\ \dfrac{d\hat{i}_{\alpha 3}}{dt} = -\dfrac{R_s}{L_{\alpha 3}}\hat{i}_{\alpha 3} + \dfrac{1}{L_{\alpha 3}}u_{\alpha 3} - \dfrac{k_2}{L_{\alpha 3}}sig\left(\hat{i}_{\alpha 3} - i_{\alpha 3}\right) \\ \dfrac{d\hat{i}_{\beta 3}}{dt} = -\dfrac{R_s}{L_{\beta 3}}\hat{i}_{\beta 3} + \dfrac{1}{L_{\beta 3}}u_{\beta 3} - \dfrac{k_2}{L_{\beta 3}}sig\left(\hat{i}_{\beta 3} - i_{\beta 3}\right) \end{cases} \tag{14}$$

where the sign function in the conventional SMO is replaced by the sigmoid function $sig(x)$ to reduce the chattering phenomenon. The sigmoid function is a continuous function and defined as:

$$sig(x) = \frac{2}{1 + \exp(-ax)} - 1 \tag{15}$$

where a is positive adjustable parameter for the slope of the sigmoid function.

Define the sliding surface as:

$$S(X) = \begin{bmatrix} s_{\alpha 1} \\ s_{\beta 1} \\ s_{\alpha 3} \\ s_{\beta 3} \end{bmatrix} = \begin{bmatrix} \tilde{i}_{\alpha 1} \\ \tilde{i}_{\beta 1} \\ \tilde{i}_{\alpha 3} \\ \tilde{i}_{\beta 3} \end{bmatrix} = \begin{bmatrix} \hat{i}_{\alpha 1} - i_{\alpha 1} \\ \hat{i}_{\beta 1} - i_{\beta 1} \\ \hat{i}_{\alpha 3} - i_{\alpha 3} \\ \hat{i}_{\beta 3} - i_{\beta 3} \end{bmatrix} \tag{16}$$

where $[s_{\alpha 1}\ s_{\beta 1}\ s_{\alpha 3}\ s_{\beta 3}]^{\mathrm{T}}$ is vector of the sliding surface; $[\tilde{i}_{\alpha 1}\ \tilde{i}_{\beta 1}\ \tilde{i}_{\alpha 3}\ \tilde{i}_{\beta 3}]^T$ represents the estimation error of the stator current in five-phase PMSM.

It can be demonstrated that the SMO is stable and converge to the sliding surface $S(X)$. In order to prove the stability of the SMO, the Lyapunov stability criteria is utilized. The Lyapunov function used to set up the existence condition of the sliding mode is considered as:

$$\begin{aligned} V_1 &= \frac{1}{2}S(X)^T S(X) = \\ &= \frac{1}{2}\left(s_{\alpha 1}^2 + s_{\beta 1}^2 + s_{\alpha 3}^2 + s_{\beta 3}^2\right) = \\ &= \frac{1}{2}\left(\tilde{i}_{\alpha 1}^2 + \tilde{i}_{\beta 1}^2 + \tilde{i}_{\alpha 3}^2 + \tilde{i}_{\beta 3}^2\right). \end{aligned} \tag{17}$$

If the designed SMO is stable and converge to the sliding surface $S(X)$, the Lyapunov function (17) should be satisfied the following conditions. First, the Lyapunov function (17) is positive definite. Second, the derivative of the Lyapunov function should be negative. As the Lyapunov function (17) is with the form of the sum of the square of the stator current error in the stationary reference frame α1-β1-α3-β3, it is obvious the Lyapunov function V_1 is positive definite. So it is only needed to prove that the derivative of the Lyapunov function is negative, i.e.

$$\begin{aligned} \dot{V}_1 &= S(X)^T \dot{S}(X) = \\ &= s_{\alpha 1}\dot{s}_{\alpha 1} + s_{\beta 1}\dot{s}_{\beta 1} + s_{\alpha 3}\dot{s}_{\alpha 3} + s_{\beta 3}\dot{s}_{\beta 3} = \\ &= \tilde{i}_{\alpha 1}\dot{\tilde{i}}_{\alpha 1} + \tilde{i}_{\beta 1}\dot{\tilde{i}}_{\beta 1} + \tilde{i}_{\alpha 3}\dot{\tilde{i}}_{\alpha 3} + \tilde{i}_{\beta 3}\dot{\tilde{i}}_{\beta 3} < 0 \end{aligned} \tag{18}$$

where $\dot{V}_1$ is the derivative of the Lyapunov function; $\dot{S}(X) = [\dot{s}_{\alpha 1}\ \dot{s}_{\beta 1}\ \dot{s}_{\alpha 3}\ \dot{s}_{\beta 3}]^T$ is derivative of the sliding surface; $[\dot{\tilde{i}}_{\alpha 1}\ \dot{\tilde{i}}_{\beta 1}\ \dot{\tilde{i}}_{\alpha 3}\ \dot{\tilde{i}}_{\beta 3}]^T$ represents the derivative of the stator current estimation error.

To prove that the derivative of the Lyapunov function is negative, the error equation of the stator current is established from (12) and (14). By subtracting (12) from (14), the error equation of the stator current is shown as:

$$\begin{cases} \dfrac{d\tilde{i}_{\alpha 1}}{dt} = -\dfrac{R_s}{L_{\alpha 1}}\tilde{i}_{\alpha 1} + \dfrac{1}{L_{\alpha 1}}e_{\alpha 1} - \dfrac{k_1}{L_{\alpha 1}}sig\left(\tilde{i}_{\alpha 1}\right) \\ \dfrac{d\tilde{i}_{\beta 1}}{dt} = -\dfrac{R_s}{L_{\beta 1}}\tilde{i}_{\beta 1} + \dfrac{1}{L_{\beta 1}}e_{\beta 1} - \dfrac{k_1}{L_{\beta 1}}sig\left(\tilde{i}_{\beta 1}\right) \\ \dfrac{d\tilde{i}_{\alpha 3}}{dt} = -\dfrac{R_s}{L_{\alpha 3}}\tilde{i}_{\alpha 3} + \dfrac{1}{L_{\alpha 3}}e_{\alpha 3} - \dfrac{k_2}{L_{\alpha 3}}sig\left(\tilde{i}_{\alpha 3}\right) \\ \dfrac{d\tilde{i}_{\beta 3}}{dt} = -\dfrac{R_s}{L_{\beta 3}}\tilde{i}_{\beta 3} + \dfrac{1}{L_{\beta 3}}e_{\beta 3} - \dfrac{k_2}{L_{\beta 3}}sig\left(\tilde{i}_{\beta 3}\right). \end{cases} \tag{19}$$

Based on the error equation of the stator current (19), the derivative of the Lyapunov function can be represented as follows:

$$\begin{aligned} \dot{V}_1 &= S(X)^T \dot{S}(X) = \\ &= \frac{1}{L_{\alpha 1}}\left[\tilde{i}_{\alpha 1}e_{\alpha 1} - k_1\tilde{i}_{\alpha 1}sig\left(\tilde{i}_{\alpha 1}\right)\right] + \\ &+ \frac{1}{L_{\beta 1}}\left[\tilde{i}_{\beta 1}e_{\beta 1} - k_1\tilde{i}_{\beta 1}sig\left(\tilde{i}_{\beta 1}\right)\right] + \\ &= \frac{1}{L_{\alpha 3}}\left[\tilde{i}_{\alpha 3}e_{\alpha 3} - k_2\tilde{i}_{\alpha 3}sig\left(\tilde{i}_{\alpha 3}\right)\right] + \\ &+ \frac{1}{L_{\beta 3}}\left[\tilde{i}_{\beta 3}e_{\beta 3} - k_2\tilde{i}_{\beta 3}sig\left(\tilde{i}_{\beta 3}\right)\right] - \\ &- \frac{R_s}{L_{\alpha 1}}\tilde{i}_{\alpha 1}^2 - \frac{R_s}{L_{\beta 1}}\tilde{i}_{\beta 1}^2 - \frac{R_s}{L_{\alpha 3}}\tilde{i}_{\alpha 1}^2 - \frac{R_s}{L_{\beta 3}}\tilde{i}_{\beta 3}^2 < 0. \end{aligned} \tag{20}$$

From the (20) and considered that all states and parameters of five-phase PMSM are bounded, the convergence condition of the SMO designed for sensorless control of five-phase PMSM is deduced as:

$$\begin{cases} k_1 > \max\left(|e_{\alpha 1}|, |e_{\beta 1}|\right) \\ k_2 > \max\left(|e_{\alpha 3}|, |e_{\beta 3}|\right). \end{cases} \tag{21}$$

It means that the SMO will be stable if the gains of the SMO meet the conditions as (21) shown. In other words, by choosing the appropriate parameters k_1 and k_2, the stability of the SMO

will be guaranteed. And the state feed-back and SMO design can be separated when the gains k_1 and k_2 are chosen properly because the SMO is with a large gain correction and the fast dynamics could be neglected. Besides, these characteristics ensure the separation principle and the global stabilization of the subsequent closed-loop control via output feedback control.

Once the system reaches the sliding surface, then

$$S(X) = \dot{S}(X) = 0 \tag{22}$$

By substituting (22) into (19), the following conditions are obtained:

$$\begin{cases} e_{\alpha 1} = k_1 sig\left(\tilde{i}_{\alpha 1}\right) \\ e_{\beta 1} = k_1 sig\left(\tilde{i}_{\beta 1}\right) \\ e_{\alpha 3} = k_2 sig\left(\tilde{i}_{\alpha 3}\right) \\ e_{\beta 2} = k_2 sig\left(\tilde{i}_{\beta 3}\right) \end{cases} \tag{23}$$

Besides, based on the error equation of the stator current (19), the convergence equation of stator current error before the system reaching sliding surface can be calculated in the following form:

$$\begin{cases} \tilde{i}_{\alpha 1} = \left[\tilde{i}_{\alpha 1}(0) - \dfrac{k_1 sig\left(\tilde{i}_{\alpha 1}\right)}{R_s}\right] e^{-\frac{R_s}{L_{\alpha 1}}t} + \dfrac{k_1 sig\left(\tilde{i}_{\alpha 1}\right) + e_{\alpha 1}}{R_s} \\ \tilde{i}_{\beta 1} = \left[\tilde{i}_{\beta 1}(0) - \dfrac{k_1 sig\left(\tilde{i}_{\beta 1}\right)}{R_s}\right] e^{-\frac{R_s}{L_{\beta 1}}t} + \dfrac{k_1 sig\left(\tilde{i}_{\beta 1}\right) + e_{\beta 1}}{R_s} \\ \tilde{i}_{\alpha 3} = \left[\tilde{i}_{\alpha 3}(0) - \dfrac{k_2 sig\left(\tilde{i}_{\alpha 3}\right)}{R_s}\right] e^{-\frac{R_s}{L_{\alpha 3}}t} + \dfrac{k_2 sig\left(\tilde{i}_{\alpha 3}\right) + e_{\alpha 3}}{R_s} \\ \tilde{i}_{\beta 3} = \left[\tilde{i}_{\beta 3}(0) - \dfrac{k_2 sig\left(\tilde{i}_{\beta 3}\right)}{R_s}\right] e^{-\frac{R_s}{L_{\beta 3}}t} + \dfrac{k_2 sig\left(\tilde{i}_{\beta 3}\right) + e_{\beta 3}}{R_s} \end{cases} \tag{24}$$

where $\left[\tilde{i}_{\alpha 1}(0)\ \tilde{i}_{\beta 1}(0)\ \tilde{i}_{\alpha 3}(0)\ \tilde{i}_{\beta 3}(0)\right]^T$ represents the initial state of the stator current estimation error in five-phase PMSM. It can be seen from (24) that the stator current estimation error is converged exponentially. And the convergence time can be calculated by ordering the estimation error of the stator current $\left[\tilde{i}_{\alpha 1}\ \tilde{i}_{\beta 1}\ \tilde{i}_{\alpha 3}\ \tilde{i}_{\beta 3}\right]^T$ equal to zero. The convergence time of the stator current estimation error is shown as:

$$\begin{cases} t_{\alpha 1} = \dfrac{L_{\alpha 1}}{R_s} \ln\left[1 - \dfrac{\tilde{i}_{\alpha 1}(0) R_s}{sig\left(\tilde{i}_{\alpha 1}\right) + e_{\alpha 1}}\right] \\ t_{\beta 1} = \dfrac{L_{\beta 1}}{R_s} \ln\left[1 - \dfrac{\tilde{i}_{\beta 1}(0) R_s}{sig\left(\tilde{i}_{\beta 1}\right) + e_{\beta 1}}\right] \\ t_{\alpha 3} = \dfrac{L_{\alpha 3}}{R_s} \ln\left[1 - \dfrac{\tilde{i}_{\alpha 3}(0) R_s}{sig\left(\tilde{i}_{\alpha 3}\right) + e_{\alpha 3}}\right] \\ t_{\beta 3} = \dfrac{L_{\beta 3}}{R_s} \ln\left[1 - \dfrac{\tilde{i}_{\beta 3}(0) R_s}{sig\left(\tilde{i}_{\beta 3}\right) + e_{\beta 3}}\right]. \end{cases} \tag{25}$$

3.2. Adaptive back EMF observer design. After the establishment of SMO, in order to achieve the sensorless control of five-phase PMSM, the rotor position and speed are needed to be estimated. So the equivalent signal of the back EMF should be obtained through the SMO. However, the equivalent signal of the back EMF from the SMO still contain high-frequency component and cannot be used for the estimation of the rotor position and speed directly. So in the conventional SMO, one or two low-pass filter is often used to the extract the required back EMF signal. Nevertheless, the insertion of low pass filters causes the phase delay which is usually compensated by the additional phase compensation module. And the introduction of low pass filters and phase compensation module makes the structure of the SMO more complex and the actual effect is not satisfactory in the PMSM sensorless control. In order to eliminate the low-pass filter and phase compensation module, an adaptive back EMF observer is designed to extract the back EMF signal for the better filtering and the estimation of the rotor speed and position.

In one estimation cycle of the rotor speed and position, the change rate of motor angular speed is far less than that of stator current. Thus the derivative of the rotor electrical angular velocity $\dot{\omega}_e$ can be considered equal to zero approximately. So the back EMF model of five-phase PMSM can be written as:

$$\begin{cases} \dfrac{de_{\alpha 1}}{dt} = -\omega_e^2 \psi_{m1} \cos\theta = -\omega_e e_{\beta 1} \\ \dfrac{de_{\beta 1}}{dt} = -\omega_e^2 \psi_{m1} \sin\theta = \omega_e e_{\alpha 1} \\ \dfrac{de_{\alpha 3}}{dt} = 0 \\ \dfrac{de_{\beta 3}}{dt} = 0. \end{cases} \tag{26}$$

Then based on the (26) and the design theory of the adaptive observer, the adaptive back EMF observer for sensorless control of five-phase PMSM is built as:

$$\begin{cases} \dfrac{d\hat{e}_{\alpha 1}}{dt} = -\hat{\omega}_e \hat{e}_{\beta 1} - l_1\left(\hat{e}_{\alpha 1} - e_{\alpha 1}\right) = -\hat{\omega}_e \hat{e}_{\beta 1} - l_1 \tilde{e}_{\alpha 1} \\ \dfrac{d\hat{e}_{\beta 1}}{dt} = -\hat{\omega}_e \hat{e}_{\alpha 1} - l_1\left(\hat{e}_{\beta 1} - e_{\beta 1}\right) = -\hat{\omega}_e \hat{e}_{\alpha 1} - l_1 \tilde{e}_{\beta 1} \\ \dfrac{d\hat{e}_{\alpha 3}}{dt} = -l_2\left(\hat{e}_{\alpha 3} - e_{\alpha 3}\right) = -l_2 \tilde{e}_{\alpha 3} \\ \dfrac{d\hat{e}_{\beta 3}}{dt} = -l_2\left(\hat{e}_{\beta 3} - e_{\beta 3}\right) = -l_2 \tilde{e}_{\beta 3} \end{cases} \tag{27}$$

where $[\hat{e}_{\alpha 1}\ \hat{e}_{\beta 1}\ \hat{e}_{\alpha 3}\ \hat{e}_{\beta 3}]^T$ is the estimation value of the back EMF of five-phase PMSM; $[\tilde{e}_{\alpha 1}\ \tilde{e}_{\beta 1}\ \tilde{e}_{\alpha 3}\ \tilde{e}_{\beta 3}]^T$ is the estimation error of the back EMF; $\hat{\omega}_e$ is the estimation value of the rotor electrical angular velocity; l_1 and l_2 are the gains of the adaptive back EMF observer which are constants determined by the stability conditions according to the Lyapunov stability criteria.

By subtracting (26) from (27), the back EMF error equation of the five-phase PMSM is

$$\begin{cases} \dfrac{d\tilde{e}_{\alpha 1}}{dt} = -\tilde{\omega}_e\hat{e}_{\beta 1} - \omega_e\tilde{e}_{\beta 1} - l_1\tilde{e}_{\alpha 1} \\ \dfrac{d\tilde{e}_{\beta 1}}{dt} = -\tilde{\omega}_e\hat{e}_{\alpha 1} - \omega_e\tilde{e}_{\alpha 1} - l_1\tilde{e}_{\beta 1} \\ \dfrac{d\tilde{e}_{\alpha 3}}{dt} = -l_2\tilde{e}_{\alpha 3} \\ \dfrac{d\tilde{e}_{\beta 3}}{dt} = -l_2\tilde{e}_{\beta 3} \end{cases} \tag{28}$$

where $\tilde{\omega}_e$ is the estimation error of the rotor electrical angular velocity and $\tilde{\omega}_e = \hat{\omega}_e - \omega_e$.

To prove the stability of the adaptive back EMF observer, the Lyapunov stability criteria is utilized. The Lyapunov function is constructed as:

$$\begin{aligned} V_2 &= \frac{1}{2}E(X)^T E(X) + \frac{1}{2\gamma}\tilde{\omega}_e^2 = \\ &= \frac{1}{2}\left(\tilde{e}_{\alpha 1}^2 + \tilde{e}_{\beta 1}^2 + \tilde{e}_{\alpha 3}^2 + \tilde{e}_{\beta 3}^2\right) + \frac{1}{2\gamma}\tilde{\omega}_e^2 \end{aligned} \tag{29}$$

where $E(X) = [\tilde{e}_{\alpha 1}\ \tilde{e}_{\beta 1}\ \tilde{e}_{\alpha 3}\ \tilde{e}_{\beta 3}]^T$, and theγ is a constant and the parameter $\gamma > 0$. So the derivative of the Lyapunov function can be represented as:

$$\begin{aligned} \dot{V}_2 &= E(X)^T\dot{E}(X) + \frac{1}{\gamma}\tilde{\omega}_e\dot{\tilde{\omega}}_e = \left(\tilde{e}_{\alpha 1}\dot{\tilde{e}}_{\alpha 1} + \tilde{e}_{\beta 1}\dot{\tilde{e}}_{\beta 1} + \right. \\ &\left. + \tilde{e}_{\alpha 3}\dot{\tilde{e}}_{\alpha 3} + \tilde{e}_{\beta 3}\dot{\tilde{e}}_{\beta 3}\right) + \frac{1}{\gamma}\tilde{\omega}_e\dot{\tilde{\omega}}_e. \end{aligned} \tag{30}$$

Since ω_e is a constant and $\tilde{\omega}_e = \hat{\omega}_e - \omega_e$, it is deduced that $\dot{\tilde{\omega}}_e = \dot{\hat{\omega}}_e$. So the derivative of the Lyapunov function can be rewritten as:

$$\begin{aligned} \dot{V}_2 &= E(X)^T\dot{E}(X) + \frac{1}{\gamma}\tilde{\omega}_e\dot{\hat{\omega}}_e = \left(\tilde{e}_{\alpha 1}\dot{\tilde{e}}_{\alpha 1} + \tilde{e}_{\beta 1}\dot{\tilde{e}}_{\beta 1} + \right. \\ &\left. + \tilde{e}_{\alpha 3}\dot{\tilde{e}}_{\alpha 3} + \tilde{e}_{\beta 3}\dot{\tilde{e}}_{\beta 3}\right) + \frac{1}{\gamma}\tilde{\omega}_e\dot{\hat{\omega}}_e. \end{aligned} \tag{31}$$

Substituting (28) into the (31), it can be deduced that,

$$\begin{aligned} \dot{V}_2 &= -l_1\left(\tilde{e}_{\alpha 1}^2 + \tilde{e}_{\beta 1}^2\right) - l_2\left(\tilde{e}_{\alpha 3}^2 + \tilde{e}_{\beta 3}^2\right) + \\ &+ \tilde{\omega}_e\left(\hat{e}_{\alpha 1}\tilde{e}_{\beta 1} - \hat{e}_{\beta 1}\tilde{e}_{\alpha 1} + \frac{1}{\gamma}\dot{\hat{\omega}}_e\right). \end{aligned} \tag{32}$$

It is obvious that the Lyapunov function of the adaptive back EMF observer is positive definite. In order to enable the designed adaptive back EMF observer stable, the derivative of the Lyapunov function of needed to be negative definite, i.e. the derivative of the Lyapunov function $\dot{V}_2$ less than zero. So the adaptive update law can be designed as:

$$\begin{cases} -l_1\left(\tilde{e}_{\alpha 1}^2 + \tilde{e}_{\beta 1}^2\right) - l_2\left(\tilde{e}_{\alpha 3}^2 + \tilde{e}_{\beta 3}^2\right) < 0 \\ \tilde{\omega}_e\left(\hat{e}_{\alpha 1}\tilde{e}_{\beta 1} - \hat{e}_{\beta 1}\tilde{e}_{\alpha 1} + \dfrac{1}{\gamma}\dot{\hat{\omega}}_e\right) = 0. \end{cases} \tag{33}$$

From (33), the adaptive update law can be easily deduced as:

$$\begin{cases} l_1 > 0 \quad \& \quad l_2 > 0 \\ \hat{\omega}_e = \gamma\int\left(\hat{e}_{\beta 1}\tilde{e}_{\alpha 1} - \hat{e}_{\alpha 1}\tilde{e}_{\beta 1}\right)dt. \end{cases} \tag{34}$$

So the rotor electrical angular velocity can be estimated as (34).

And the estimation value of rotor position can be expressed as:

$$\hat{\theta} = -\arctan\left(\frac{\hat{e}_{\alpha 1}}{\hat{e}_{\beta 1}}\right) \tag{35}$$

3.3. Iterative sliding mode observer design. As the adaptive back EMF observer eliminates the low-pass filter and phase compensation module, the total computational cost of the new SMO is lower than the conventional SMO. However, for the high speed sensorless control of five-phase PMSM, the large gains are needed for the SMO to reduce the response time. Nevertheless, the large gains of the SMO will aggravate the chattering phenomenon in the whole speed regulation process and the estimation process of the rotor position and the rotor electrical angular velocity. Therefore, it is necessary to adjust the gains of the SMO within a certain range in low and high speed stages to further reduce the chattering during the estimation process. So the ISMO is designed to reduce the chattering by iterative adjustment of the sliding mode gains during the speed regulation process and the estimation process.

Figure 4 is the schematic of the proposed ISMO. The ISMO proposed for sensorless control of five-phase PMSM divides one control period of the stator current into three parts between two times of the actual current sampling and adds two times of virtual current sampling for the iterative calculation of the sliding mode gains.

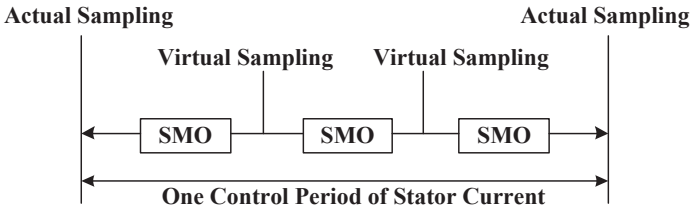

Fig. 4. Schematic of the ISMO for five-phase PMSM sensorless control

The block diagram of ISMO for sensorless control of five-phase PMSM is shown as Fig. 5. The sliding mode gains are adjusted appropriately in each virtual current sampling to reduce chattering and ensure the adjusted sliding mode gains are satisfied the stability condition. The number of the iterative calculation for the sliding mode gains is only three times because the new SMO is with two sliding mode gains, and with the each addition of iterative calculation for sliding mode gains, the amount of calculations in the whole sensorless control system of five-phase PMSM will increase sharply. So in one current control cycle, three times iterative calculations with different sliding mode gains in sensorless control system of five-phase PMSM is maximally allowed by the actual applied microprocessor. And the sliding mode gains are adjusted from a relatively higher value to a relatively lower value in each current control cycle to reduce the ripples in the speed regulation process and the estimation process.

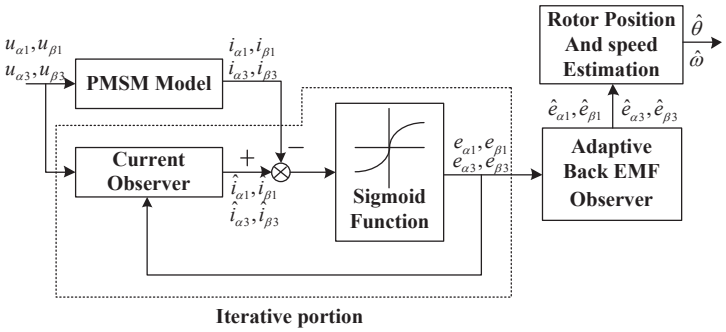

Fig. 5. Black diagram of ISMO for sensorless control of five-phase PMSM

4. Experiment verification

In order to verify the effectiveness of the proposed ISMO for sensorless control of five-phase PMSM in electric drive system, the simulation experiment platform is built as Fig. 1 shown. The five-phase PMSM is coupled with load generation unit which is used to measure torque and give a load torque. The controller is with the digital SVPWM generator to realize the sensorless control strategy. The simulation experiment data is recorded and saved by LabVIEW-based data acquisition system and transformed by Matlab. To compare the performance of proposed ISMO with conventional SMO, the experiments are done under the conditions of rated speed and rated load torque based on proposed ISMO and conventional SMO with third harmonic firstly. In addition, to test the performance of proposed ISMO for sensorless control of five-phase PMSM in electric drive system even further, the experiments are done under different operating conditions, such as low speed, high speed, speed inversion, step and inversion load torque. The parameters of five-phase PMSM in electric drive system are shown in Table 1 and the related parameters of ISMO for sensorless control are shown in Table 2.

Table 1
Parameters of five-phase PMSM in electric drive system

Parameter	Symbol	Value
Stator winding resistance	R_s	0.12 Ω
Fundamental component of stator inductance in stationary reference frame	$L_{\alpha1}$, $L_{\beta1}$	1.35 mH
Third harmonic component of stator inductance in stationary reference frame	$L_{\alpha3}$, $L_{\beta3}$	0.034 mH
Flux amplitude of fundamental wave	Ψ_{m1}	0.05 Wb
Moment of inertia	J	0.002 kgm^2
Friction constant	B	0.02 Nms
Number of pole pairs	P	4
Rated load torque	T_L	11 Nm
Rated power	P_w	4.4 kW
Rated speed	ω	900 r/min

Table 2
Parameters of ISMO for sensorless control

Parameter	Symbol	Value
Initial sliding mode current observer gain of fundamental component	k_1	100
Initial sliding mode current observer gain of third harmonic component	k_2	40
Adaptive back EMF observer gain of fundamental component	l_1	500
Adaptive back EMF observer gain of third harmonic component	l_2	200
Slope of the sigmoid function	a	1
Adjustment coefficient of Lyapunov function for adaptive back EMF observer	γ	1

Figure 6 shows the waveforms of conventional SMO under rated speed and rated load torque. Figure 7 is the waveforms of ISMO under rated speed and rated load torque. Both the conventional SMO and the proposed ISMO are tested under the same condition. The reference speed is 900 r/min and the speed ramps of acceleration and deceleration are ±16.7 r/s^2. At 1.2 s, the load torque is stepped to 11 Nm. Compared the speed wave in Fig. 6(a) with the one in Fig. 7(a), it can be seen that the chattering in the rotor speed estimation of conventional SMO with sign function is larger the one of proposed ISMO with sigmoid function. And compared the other waves in Fig. 6 with the ones in Fig. 7, the chattering in the estimations of rotor position, fundamental of back EMF and third harmonic of back EMF are as the same cases. And by calculation, the maximum error of the rotor speed estimation in proposed ISMO is approximately 0.1% in transients and it converges to zero in the steady state, while the maximum error of the rotor speed estimation in conventional SMO is approximately 0.5%. Besides, the maximum

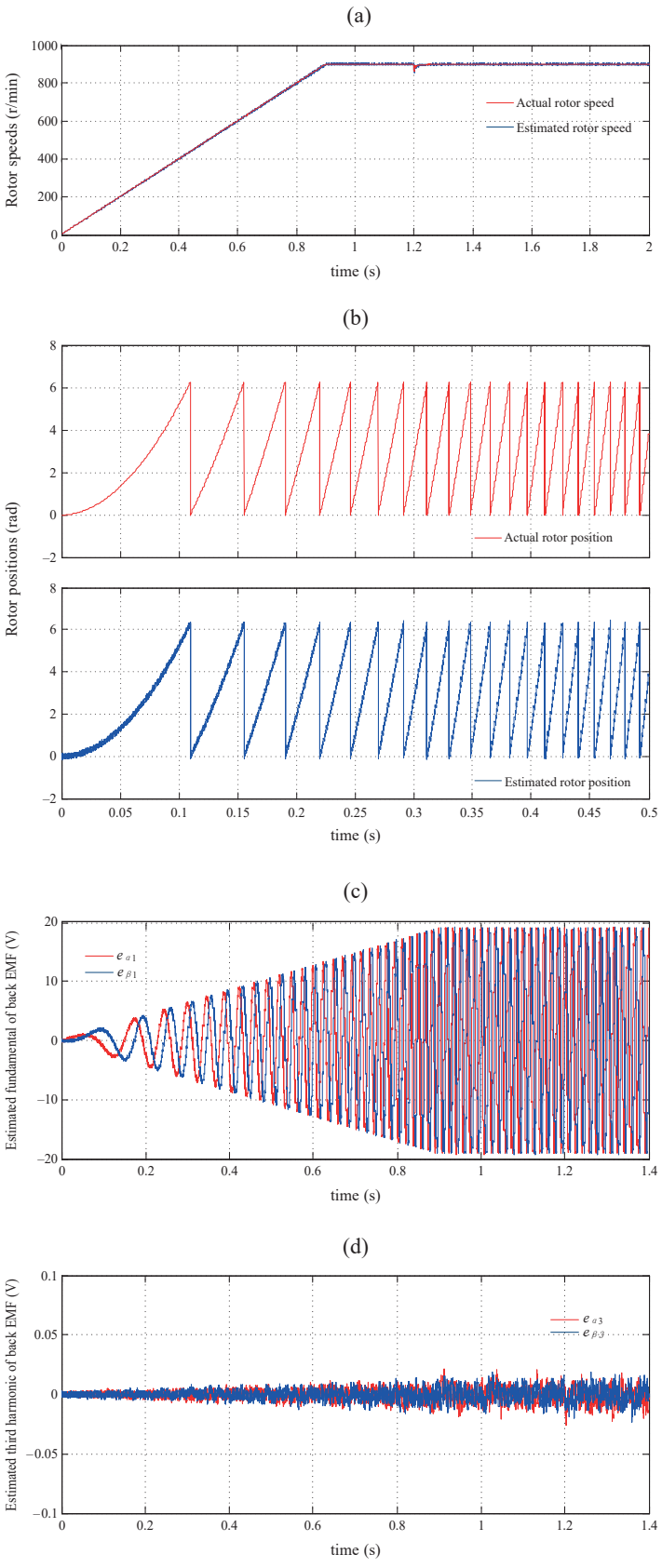

Fig. 6. Waveforms of conventional SMO under rated speed and rated load torque condition: a) Actual and estimated rotor speeds; b) Actual and estimated rotor positions; c) Estimated fundamental of back EMF; d) Estimated third harmonic of back EMF

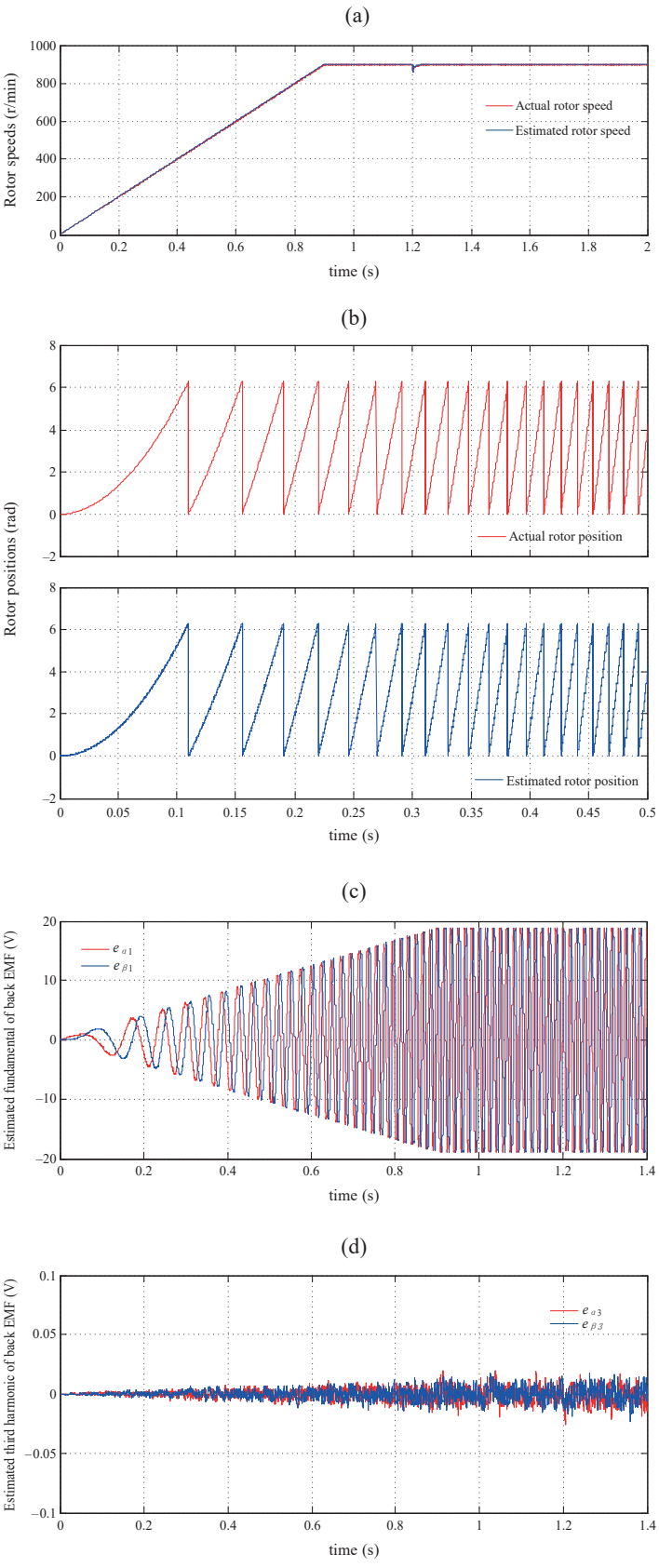

Fig. 7. Waveforms of ISMO under rated speed and load torque condition: a) Actual and estimated rotor speeds; b) Actual and estimated rotor positions; c) Estimated fundamental of back EMF; d) Estimated third harmonic of back EMF

error of the rotor position estimation in proposed ISMO is approximately 0.05% owing to the continuous transformation of the position signal between each 2π radian, while the maximum error of the rotor position estimation in conventional ISMO is approximately 0.1%.

Figure 8 shows the waveforms of ISMO under low speed condition. The reference speed is 50 r/min and the speed ramps of acceleration and deceleration are also ±16.7 r/s^2. At 0.1s, the load torque is stepped to 11 Nm. From Fig. 8, it is obvious that the proposed ISMO is with good performance on rotor speed and position tracking, and back EMF estimation at low speed condition. The load disturbance has no significant impact on the overall estimation process. And due to the calculation, the maximum error of the rotor speed estimation in proposed ISMO is approximately 0.15% in transients and the maximum error of the rotor position estimation is approximately 0.06%.

Figure 9 shows the waveforms of ISMO under high speed condition. The reference speed is 1200 r/min. At 1.5 s, the load torque is stepped to 11 Nm. From Fig. 9, it is clear that the proposed ISMO is also with good performance on rotor speed and position tracking, and back EMF estimation at high speed condition. The load disturbance also has no obvious impact on the overall estimation process. And from the calculation, the maximum error of the rotor speed estimation in proposed ISMO is approximately 0.3% in transients and the maximum error of the rotor position estimation is approximately 0.08%. From Fig. 7 to Fig. 9, it proves that the proposed ISMO for five-phase PMSM is with good speed control ability in sensorless control.

Furthermore, in order to verify the robustness of the proposed ISMO against the disturbance, the speed and load mutation status are taken into account. Figure 10 is the waveforms of ISMO under speed inversion condition. The initial reference speed is 900 r/min. At 0.95 s, the load torque is stepped to 11 Nm. At 1.05 s, the reference speed is stepped to −900 r/min and the speed ramps of acceleration and deceleration are still ±16.7 r/s^2. From Fig. 10, it can be seen that the proposed ISMO is still with outstanding performance on the estimation of the rotor speed, position and back EMF under speed inversion condition. The sudden change of reference speed also has no significant effect in the overall tracking process. Based on the calculation, the maximum error of the rotor speed estimation in proposed ISMO is approximately 0.2% at 0.95 s when the load torque is stepped to 11 Nm, and the maximum error of the rotor position estimation is also approximately 0.05%.

Figure 11 shows the waveforms of ISMO under step and inversion load torque condition. The reference speed is still 900 r/min. At 1.2 s, the load torque is stepped to 11 Nm. At 1.5 s, the load torque is stepped to −11 Nm. From Fig. 11, it is illustrated that the proposed ISMO is still with excellent performance on rotor speed, position and back EMF estimation under load torque inversion condition. The sudden reverse of load torque also has no obvious effect in the overall estimation process. From the calculation, the maximum error of the rotor speed estimation in proposed ISMO is approximately 0.3% at 1.5 s when the load torque is stepped to −11 Nm, and the maximum error of the rotor position estimation is also approx-

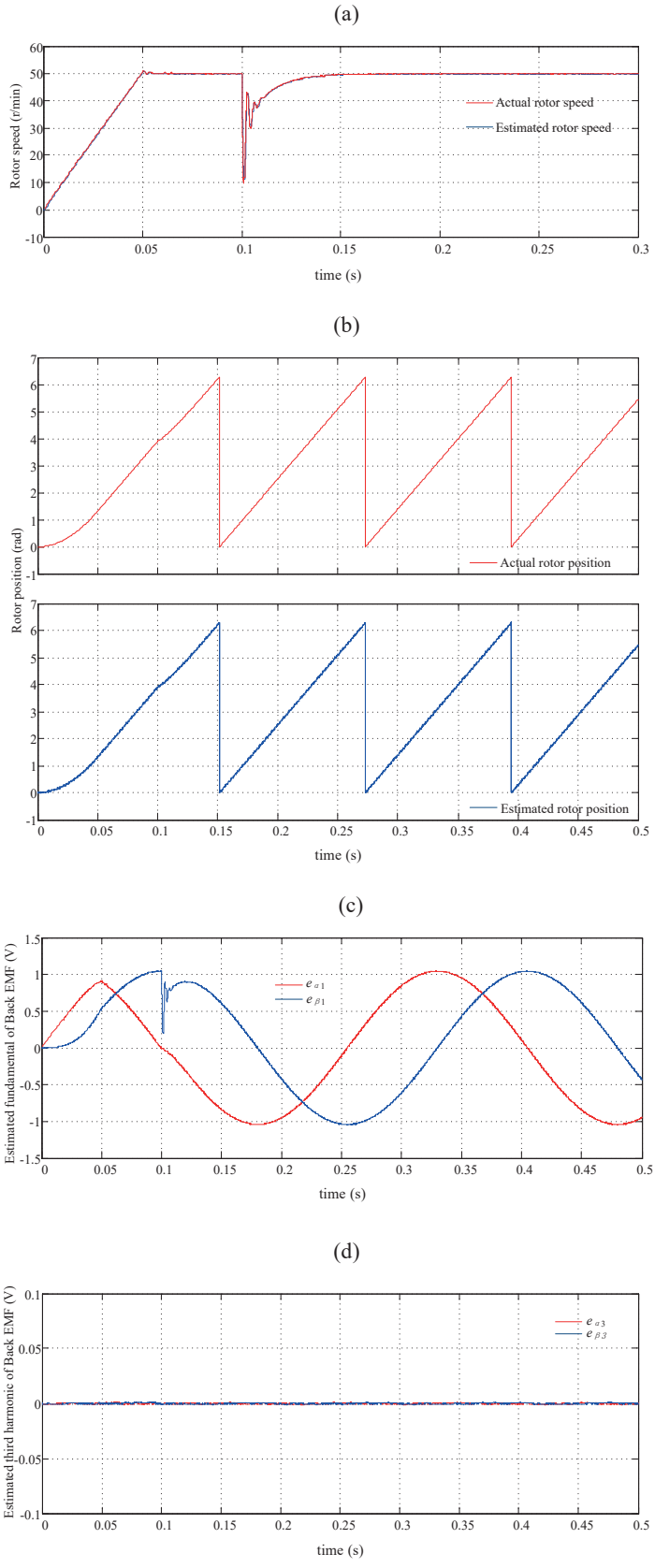

Fig. 8. Waveforms of ISMO under low speed condition: a) Actual and estimated rotor speeds; b) Actual and estimated rotor positions; c) Estimated fundamental of back EMF; d) Estimated third harmonic of back EMF

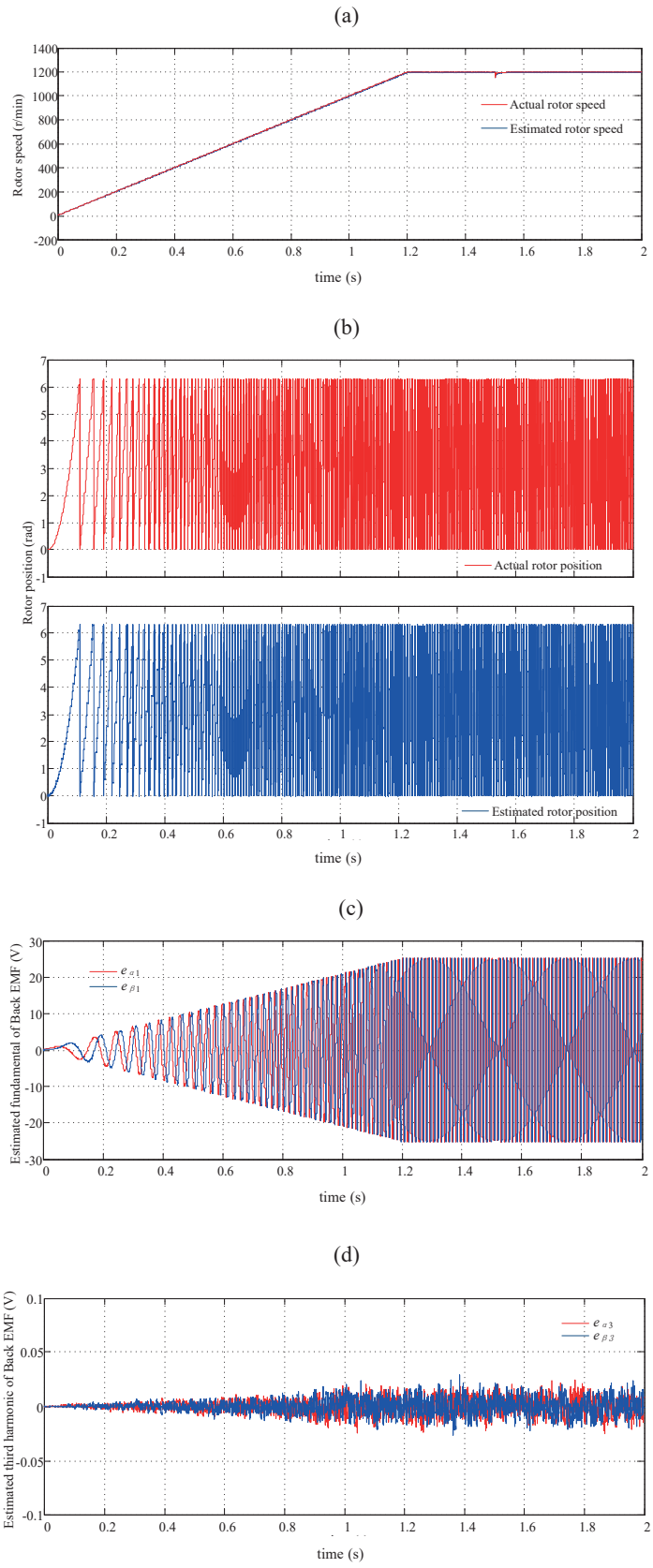

Fig. 9. Waveforms of ISMO under high speed condition: a) Actual and estimated rotor speeds; b) Actual and estimated rotor positions; c) Estimated fundamental of back EMF; d) Estimated third harmonic of back EMF

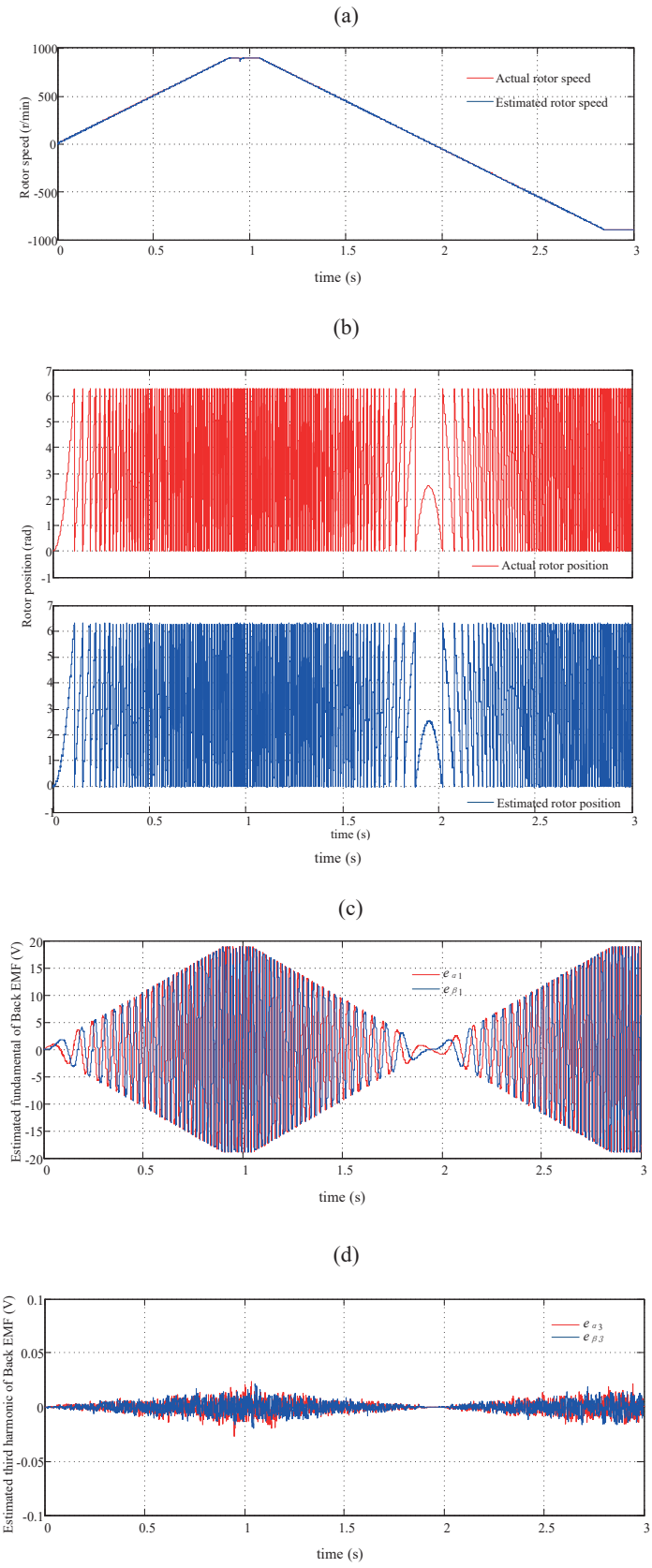

Fig. 10. Waveforms of ISMO under speed inversion condition: a) Actual and estimated rotor speeds; b) Actual and estimated rotor positions; c) Estimated fundamental of back EMF; d) Estimated third harmonic of back EMF

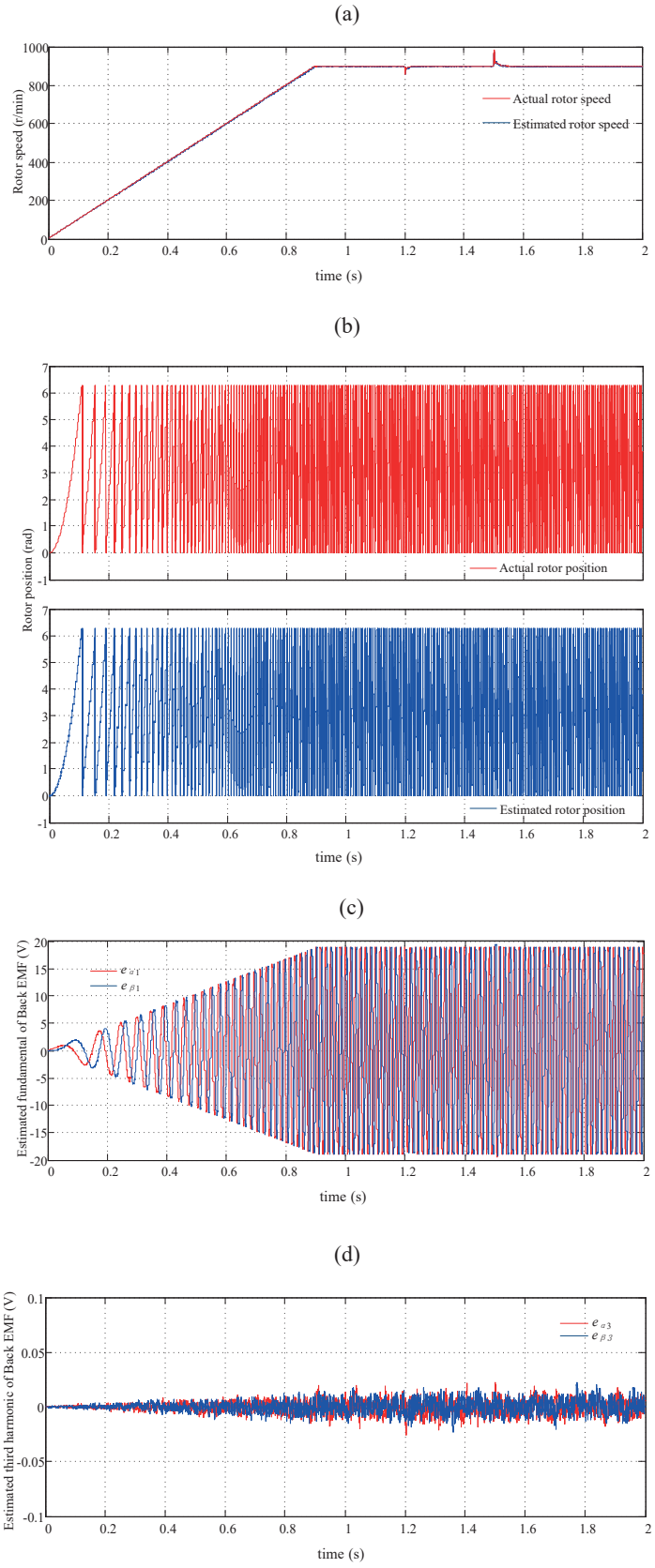

Fig. 11. Waveforms of ISMO under step and inversion load torque condition: a) Actual and estimated rotor speeds; b) Actual and estimated rotor positions; c) Estimated fundamental of back EMF; d) Estimated third harmonic of back EMF

imately 0.06%. From Fig. 10 and Fig. 11, it verifies that the proposed ISMO for five-phase PMSM is with good robustness against the disturbances in sensorless control.

5. Conclusions

In this paper, a new ISMO is proposed for sensorless control of five-phase PMSM with the consideration of the impact of the third harmonic. A SMO is designed firstly based on the five-phase PMSM model with the third harmonic to reduce the chattering and obtain the equivalent signal of the back EMF. And then, the adaptive observer of back EMF is built to estimate the rotor speed and the rotor position of five-phase PMSM, which eliminates the low-pass filter and phase compensation module and improves the estimation accuracy. Simultaneously, by iteratively using the SMO in one current sampling period to adjust the sliding mode gains, the sliding mode chattering and estimation errors of motor speed and angle are further reduced. Besides, the stability of the SMO and the adaptive back EMF observer is demonstrated in detail by Lyapunov stability criteria. The experiment results show that the proposed ISMO is with smaller chattering than conventional SMO. Besides, the speed control ability and robustness against the disturbances are also excellent, which verifies the feasibility and effectiveness of the proposed observer for five-phase PMSM sensorless control.

Acknowledgements. This work was supported by the National Natural Science Foundation of China (Grant no. 51507143), Specialized Research Fund for the Doctoral Program of Higher Education of China (Grant no. 20136102120055), and the Industry Science and Technology Research Foundation of Shaanxi Province, China (Grant no. 2015GY090).

References

[1] A. Mohammadpour, and L. Parsa, "Global fault-tolerant control technique for multiphase permanent-magnet machines", *IEEE Trans. Ind. Appl.* 51 (1), 178–186 (2015).

[2] M. Janaszek, "Structures of vector control of n-phase motor drives based on generalized Clarke transformation", *Bull. Pol. Ac.: Tech.* 64 (4), 865–872 (2016).

[3] N.K. Nguyen, F. Meinguet, E. Semail, and X. Kestelyn, "Fault-tolerant operation of an open-end winding five-phase PMSM drive with short-circuit inverter fault", *IEEE Trans. Ind. Electron.* 63 (1), 595–605 (2016).

[4] A. Mohammadpour, S. Sadeghi, and L. Parsa, "A generalized fault-tolerant control strategy for five-phase PM motor drives considering star, pentagon, and pentacle connections of stator windings", *IEEE Trans. Ind. Electron.* 61 (1), 63–75 (2014).

[5] A. Mohammadpour and L. Parsa, "A unified fault-tolerant current control approach for five-phase PM motors with trapezoidal back EMF under different stator winding connections", *IEEE Trans. Power Electron.* 28 (7), 3517–3527 (2013).

[6] S. Sadeghi, L. Guo, H.A. Toliyat, and L. Parsa, "Wide operational speed range of five-phase permanent magnet machines by using different stator winding configurations", *IEEE Trans. Power Electron.* 59 (6), 2621–2631 (2012).

[7] L. Guo and L. Parsa, "Model reference adaptive control of five-phase IPM motors based on neural network", *IEEE Trans. Ind. Electron.* 59 (3), 1500–1508 (2012).

[8] N. Leboeuf, T. Boileau, B. Nahid-Mobarakeh, N. Takorabet, F. Meibody-Tabar, and G. Clerc, "Effects of imperfect manufacturing process on electromagnetic performance and online interturn fault detection in pmsms", *IEEE Trans. Ind. Electron.* 62 (6), 3388–3398 (2015).

[9] M. Trabelsi, N.K. Nguyen, and E. Semail, "Real-time switches fault diagnosis based on typical operating characteristics of five-Phase permanent-magnetic synchronous machines", *IEEE Trans. Ind. Electron.* 63 (8), 4683–4694 (2016).

[10] F. Betin, G.A. Capolino, D. Casadei, B. Kawkabani, R.I. Bojoi, L. Harnefors, E. Levi, L. Parsa, and B. Fahimi "Trends in electrical machines control: samples for classical, sensorless, and fault-tolerant Techniques", *IEEE Trans. Ind. Electron.* 8 (2), 43–55 (2014).

[11] B. Alecsa, M.N. Cirstea, and A. Onea, "Simulink modeling and design of an efficient hardware-constrained FPGA-based PMSM speed controller", *IEEE Trans. Ind. Informat.* 8 (3), 554–562 (2012).

[12] Q. Tang, A. Shen, X. Luo, and J. Xu, "PMSM sensorless control by injecting HF pulsating carrier signal into ABC frame", *IEEE Trans. Power Electron.* 32 (5), 3767–3776 (2017).

[13] X. Song, J. Fang, B. Han, and S. Zheng, "Adaptive compensation method for high-speed surface PMSM sensorless drives of EMF-based position estimation error", *IEEE Trans. Power Electron.* 31 (2), 1438–1449 (2016).

[14] T. Atalik, M. Deniz, E. Koc, C. Gercek, B. Gultekin, M. Ermis, and I. Cadirci, "Multi-DSP and FPGA based fully-digital control system for cascaded multilevel converters used in FACTS applications", *IEEE Trans. Ind. Informat.* 8 (3), 511–527 (2012).

[15] A. Al Nabulsi and R. Dhaouadi, "Efficiency optimization of a DSP-based standalone PV system using fuzzy logic and dual-MPPT control", *IEEE Trans. Ind. Informat.* 8 (3), 573–584 (2012).

[16] C. Buccella, C. Cecati, and H. Latafat, "Digital control of power converters-A survey", *IEEE Trans. Ind. Informat.* 8 (3), 437–447 (2012).

[17] X. Luo, Q.P. Tang, A.W. Shen, and Q. Zhang, "PMSM Sensorless control by injecting HF pulsating carrier signal into estimated fixed-frequency rotating reference frame", *IEEE Trans. Ind. Electron.* 63 (4), 2294–2303 (2016).

[18] M. Ramezani and O. Ojo, "The modeling and position-sensorless estimation technique for A nine-phase interior permanent-magnet machine using high-frequency injections", *IEEE Trans. Ind. Appl.* 52 (2), 1555–1565 (2016).

[19] A. Accetta, M. Cirrincione, M. Pucci, and G. Vitale, "Sensorless control of PMSM fractional horsepower drives by signal injection and neural adaptive-band filtering", *IEEE Trans. Ind. Electron.* 59 (3), 1355–1366 (2012).

[20] G. Wang, L. Ding, Z.M. Li, J. Xu, G.Q. Zhang, H.L. Zhan, R.G. Ni, and D.G. Xu, "Enhanced position observer using second-order generalized integrator for sensorless interior permanent magnet synchronous motor drives", *IEEE Trans. Ener. Conv.* 29 (2), 486–495 (2014).

[21] F.J. Lin, Y.C. Hung, J.M. Chen, and C.M. Yeh, "Sensorless IPMSM drive system using saliency back-EMF-based intelligent torque observer with MTPA control", *IEEE Trans. Ind. Informat.* 10 (2), 1226–1241 (2014).

[22] G.L. Wang, H.L. Zhan, G.Q. Zhang, X.G. Gui, and D.G. Xu, "Adaptive compensation method of position estimation harmonic error for EMF-based observer in sensorless IPMSM drives", *IEEE Trans. Power Electron.* 26 (6), 3055–3064 (2014).

[23] H.X. Liu and S.H. Li, "Speed control for PMSM servo system using predictive functional control and extended state observer", *IEEE Trans. Ind. Electron.* 59 (2), 1171–1183 (2012).

[24] R. Errouissi, M. Ouhrouche, W.-H. Chen, and A.M. Trzynadlowski, "Robust nonlinear predictive controller for a PMSM with optimized cost function", *IEEE Trans. Ind. Electron.* 59 (7), 2849–2858 (2012).

[25] N.K. Quang, N.T. Hieu, and Q.P. Ha, "FPGA-based sensorless PMSM speed control using reduced-order extended Kalman filters", *IEEE Trans. Ind. Electron.* 61 (12), 6574–6582 (2014).

[26] K. Zawirski, D. Janiszewski, and R. Muszynski, "Unscented and extended Kalman filters study for sensorless control of PM synchronous motors with load torque estimation", *Bull. Pol. Ac.: Tech*. 61 (4), 793–801 (2013).

[27] H. Lee and J. Lee, "Design of iterative sliding mode observer for sensorless PMSM control", *IEEE Trans. on Control Syst. Technol.* 21 (4), 1394–1399 (2013).

[28] Z.W. Qiao, T.N. Shi, Y.D. Wang, Y.Yan, C.L. Xia, and X.N. He "New sliding-mode observer for position sensorless control of permanent-magnet synchronous Motor", *IEEE Trans. Ind. Electron.* 60 (2), 710–719 (2013).

[29] S.H. Li, M.M. Zhou, and X.H. Yu, "Design and implementation of terminal sliding mode control method for PMSM speed regulation system", *IEEE Trans. Ind. Inf.* 9 (4), 1879–1891 (2012).

[30] G.L. Wang, T.L. Li, G.Q. Zhang, X.G. Gui, and D.G. Xu, "Position estimation error reduction using recursive-least-square adaptive filter for model-based sensorless interior permanent-magnet synchronous motor drives", *IEEE Trans. Ind. Electron.* 61 (9), 5115–5125 (2014).

[31] Y. Gao, W.G Liu, and Q. Yang, "Study of position sensorless control based on sliding mode observer", in proc. *International conference on electrical machines and systems (ICEMS)*, 1–3 (2011).

[32] J.W. Yang, M.F. Dou, Z.Y. Dai, D.D. Zhao, and Z. Zhang, "Modeling and fault diagnosis of inter-turn short circuit for five-phase PMSM based on particle swarm optimization", in Proc. *IEEE Appl. Power Electron. Conf. Expo.* 3134–3139 (2016).

[33] W.C. Chi and M.Y. Cheng, "Implementation of a sliding-mode-based position sensorless drive for high-speed micro permanent-magnet synchronous motors", *ISA Trans.* 53 (2), 444–453 (2014).

[34] D. Xu, S.G. Zhang, and J.M. Liu, "Very-low speed control of PMSM based on EKF estimation with closed loop optimized parameters", *ISA Trans.* 52 (6), 835–843 (2013).